Structural transitions in the FixJ receiver domain

Patrice Gouet[1], Béatrice Fabry[1], Valérie Guillet[1], Catherine Birck[1], Lionel Mourey[1], Daniel Kahn[2] and Jean-Pierre Samama[1]*

Background: Two-component signal transduction pathways are sophisticated phosphorelay cascades widespread in prokaryotes and also found in fungi, molds and plants. FixL/FixJ is a prototypical system responsible for the regulation of nitrogen fixation in the symbiotic bacterium *Sinorhizobium meliloti*. In microaerobic conditions the membrane-bound kinase FixL uses ATP to transphosphorylate a histidine residue, and the response regulator FixJ transfers the phosphoryl group from the phosphohistidine to one of its own aspartate residues in a Mg^{2+}-dependent mechanism.

Results: Seven X-ray structures of the unphosphorylated N-terminal receiver domain of FixJ (FixJN) have been solved from two crystal forms soaked in different conditions. Three conformations of the protein were found. In the first case, the protein fold impairs metal binding in the active site and the structure reveals a receiver domain that is self-inhibited for catalysis. In the second conformation, the canonical geometry of the active site is attained, and subsequent metal binding to the protein induces minimal conformational changes. The third conformation illustrates a non-catalytic form of the protein where unwinding of the N terminus of helix α1 has occurred. Interconversion of the canonical and self-inhibited conformations requires a large conformational change of the β3–α3 loop region.

Conclusions: These unphosphorylated structures of FixJN stress the importance of flexible peptide segments that delineate the active site. Their movements may act as molecular switches that define the functional status of the protein. Such observations are in line with structural and biochemical results obtained on other response regulator proteins and may illustrate general features that account for the specificity of protein–protein interactions.

Addresses: [1]Groupe de Cristallographie Biologique, CNRS-IPBS, 205 route de Narbonne, 31077-Toulouse, France and [2]Laboratoire de Biologie Moléculaire des Relations Plantes-Microorganismes, UMR 215 INRA-CNRS, Chemin de Borde Rouge, BP27, Castanet-Tolosan CEDEX, France.

*Corresponding author.
E-mail: samama@ipbs.fr

Key words: conformational changes, nitrogen-fixation regulation, protein–protein interface, response regulator, X-ray structure

Received: 11 September 1999
Revisions requested: 1 October 1999
Revisions received: 1 November 1999
Accepted: 2 November 1999

Published: 26 November 1999

Structure December 1999, 7:1517–1526

0969-2126/99/$ – see front matter

Introduction

A large variety of adaptative cellular responses to environmental stimuli, such as osmoregulation, sporulation, pathogenicity and chemotaxis [1] are mediated by two-component systems [2]. These signaling cascades are widespread in bacteria and are also found in lower eukaryotic organisms [3–5]. They involve two essential protein families, the sensor histidine kinases and the response regulator proteins. On detecting a stimulus, the sensor protein, which may be an input domain of the kinase itself or a receptor coupled to it, modulates the activity of the transmitter module of the kinase. Signal transduction is mediated by Mg^{2+}-dependent phosphorelay reactions between the kinase and the phosphoaccepting receiver domain of the cognate response regulator protein.

The FixL/FixJ two-component system is responsible for the regulation of nitrogen fixation in the symbiotic bacterium *S. meliloti* [6,7]. The membrane-bound kinase FixL contains an oxygen-sensing domain and a transmitter module. In microaerobic conditions this module uses ATP to transphosphorylate a histidine residue conserved in the kinase family [8,9]. The phosphoryl group is then transferred to a conserved aspartate residue on the N-terminal regulatory, or receiver domain, of the FixJ response regulator, which displays a typical two-domain arrangement [10,11]. Phosphorylation of the receiver domain mediates dimerization of the protein [12,13] and relieves the inhibition of the C-terminal domain as transcriptional activator of the *nifA* and *fixK* genes [14–16].

Sequence and structure homologies between receiver domains suggested a common Mg^{2+}-dependent mechanism of phosphorylation for all members of the response regulator superfamily [17–19]. The structures exhibit a common $(\beta/\alpha)_5$ fold [18,20–26], and similar active sites where three invariant residues are located (Asp11, Asp54 and Lys104 in FixJ). Phosphorylation of Asp54 in FixJ induces a cascade of conformational changes; these were revealed by the X-ray structure of the phosphorylated receiver domain [13].

In vivo the production of the output response is highly regulated by the number of phosphorylated species. Their formation involves a selective recognition of the receiver domain by the cognate kinase and it was also proposed that the ability of this domain to bind the essential metal ion in the active site could be a means of modulating the functional status of the response regulator [24]. In this paper, we report seven X-ray structures of the unphosphorylated N-terminal receiver domain of FixJ (FixJN), with and without bound metal cations, at a maximum resolution of 1.6 Å. These structures, solved from crystals grown and soaked in different conditions, provide snapshots of the conformational states of FixJN. Leu55, the residue adjacent to the phosphorylatable aspartic acid, and loop β3–α3 play a central role in the observed conformational changes of the protein.

Results and discussion

Overview of the crystal structures

The topology of FixJN is described by a doubly wound five-stranded β/α fold where the parallel β sheet is sandwiched by helices α1 and α5 on one side and helices α2, α3 and α4 on the other side (Figure 1a,b). The protein core is made of strands β1, β3 and β4, which are lined by conserved hydrophobic residues [19]. The C-terminal ends of these strands and their connecting loops to the following helices (β1–α1, β3–α3 and β4–α4) define the active-site depression. The polypeptide stretch (residues 55–61) connecting strand β3 to helix α3, known as the γ loop [19], displays two significantly different conformations (Figure 1a). One of them has never been observed in the structures of other receiver domains and its fold impairs metal binding in the active site. The two structures of FixJN where this conformation is found were called 'self-inhibited' and 'atypical'. In the latter, unwinding of the N terminus of helix α1 up to Ser18 also occurs. The second conformation of the γ loop yields the 'canonical' structure of FixJN. The receiver domain displays a proper geometry of the active site for metal binding and, accordingly, subsequent binding of this ion induced minimal structural changes. Table 1 summarizes the occurrence of the three FixJN structures in the two crystal forms. It shows that two different species may be simultaneously present in one asymmetric unit, which indicates

Figure 1

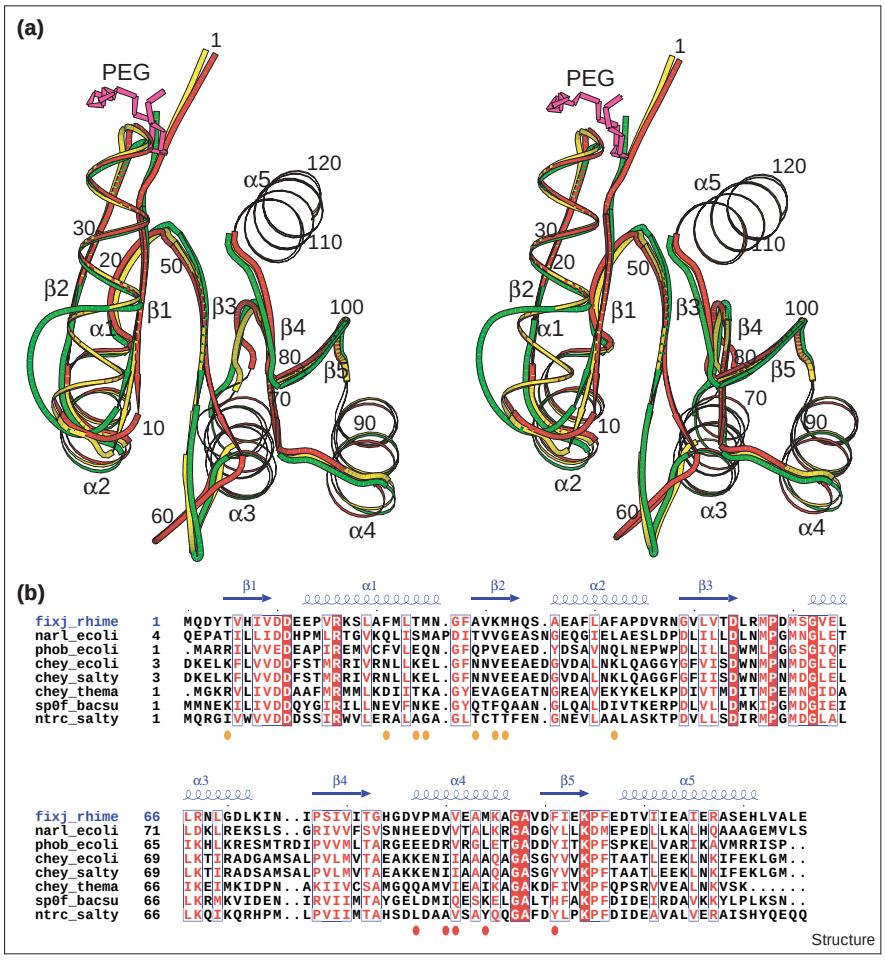

(a) Stereoview of the three FixJN unphosphorylated structures (red, canonical; yellow, self-inhibited; green, atypical). The γ loop region (residues 55–61) connects strand β3 to helix α3. The secondary structure elements and every tenth residue are indicated. The bound PEG fragment is shown in magenta. (b) Structure-based sequence alignment of FixJN and of receiver domains of known structure: *S. meliloti* FixJN (this work), *E. coli* NarL [23], *E. coli* PhoB [26], *E. coli* CheY [56], *S. typhimurium* CheY [18], *T. maritima* CheY [35], *B. subtilis* Spo0F [22,24], and *S. typhimurium* NtrC [21]. The secondary structure elements of FixJN are indicated by coils for α helices and arrows for β sheets. Homologous residues are in red and identical residues are shown as white letters on a red background. Residues of FixJN involved in the β1–α1–β2–α2, and in the α4–β5 interfaces are indicated by yellow and red dots, respectively. The figure was created using ESPript [57].

Table 1

Occurrence of the three FixJN conformations in the two crystal forms and their refinement statistics.

Crystal forms	Triclinic					Monoclinic	
Structures	FixJN	FixJN–$PtCl_4^{2-}$	FixJN–Sm^{3+}	FixJN–Mn^{2+}	FixJN–Mg^{2+}	FixJN	FixJN–Mn^{2+}
Resolution (Å)	15–1.6	15–1.9	15–2.4	15–2.0	15–2.0	15–2.9	15–3.0
No. of copies in AU*	2(Sl-C)†	2(Sl-Sl)	2(C-C)	2(C-C)	2(C-C)	2(Sl-Sl)	2(C-A)
No. of reflections	20,600	15,961	8,245	12,977	13,448	5,363	4,663
R factor (R_{free}) (%)	18.6 (22.2)	21.9 (26.8)	19.6 (26.5)	20.6 (25.3)	21.9 (27.4)	23.1 (29.2)	25.3 (33.6)
Rmsd bond lengths (Å)	0.012	0.012	0.011	0.012	0.012	0.010	0.010
Rmsd bond angles (°)	1.7	1.6	1.7	1.6	1.6	1.4	1.6
Nonhydrogen atoms	2,040	1,836	1,951	1,995	1,969	1,920	1,785
Heteroatoms	148 H_2O PEG‡	71 H_2O, 4 Pt^{2+}, 4Cl^-	75 H_2O, PEG‡, 4 Sm^{3+}	94 H_2O, PEG‡, 3 Mn^{2+}	91 H_2O, PEG‡, 2 Mg^{2+}	34 H_2O	12 H_2O 1 Mn^{2+}
Average B ($Å^2$)	22	25	22	26	27	14	57

*AU is asymmetric unit. †Sl, self-inhibited; C, canonical; A, atypical. ‡Ordered segment of 19 atoms of PEG 1500 has been modeled as -O-(CH2CH2O)$_6$-.

that the crystallization processes did not select one population. Soaking the crystals in solutions of metal ions (Sm^{3+}, Mn^{2+} or Mg^{2+}) induced the conformational change from the self-inhibited to the canonical structure, except in one case where it led to the atypical structure. In contrast, soaking with platinum chloride ($PtCl_4^{2-}$) favored the self-inhibited structure over the canonical one (Table 1). The superposition of the self-inhibited and canonical structures of the asymmetric unit in the native triclinic crystals gave a root mean square deviation (rmsd) value of 0.7 Å for all C_α pairs when excluding residues 55–61 from the calculation. On the basis of this superposition, the γ loop regions differ by an rmsd value of 3.0 Å. Apart from the protein–protein contacts leading to the major interfaces described below, one crystal-packing interaction is observed in all triclinic crystals. Loops α2–β3 and α3–β4 from a symmetry-related self-inhibited molecule are in the vicinity of the His84 sidechain and of the α1–β5–α5 area of the canonical molecule, respectively. Both molecules undergo conformational changes (Table 1), suggesting that these packing contacts do not affect the structures. In the triclinic crystals, a continuous electron density was assigned to 19 atoms of a polyethylene glycol (PEG) fragment bound in a pocket lined by residues from two adjacent molecules (Figure 2). Three oxygen atoms of the ether groups interact with the amino group of a lysine sidechain, and the conformation of this fragment is close to that of a crown polyether with a cationic group at its center [27]. The binding of a PEG molecule in crystal structures has only been reported for the peptide deformylase enzyme from *Escherichia coli* [28] and for the human peptidyl-prolyl *cis–trans* isomerase Pin1 [29].

The canonical structure

The active site of the receiver domain of FixJ comprises the conserved Asp10, Asp11 and Asp54 residues (Figure 3). Glu12 is oriented towards this acidic pocket, as is the invariant Lys104 from the β5–α5 loop. Lys104 makes no direct interaction with any of the acidic groups. A water molecule is found in the active site at hydrogen-bonding distance (2.5 Å) from the mainchain oxygen atom of residue 56 and the carboxylic oxygen atoms of Asp11 and Asp54. Leu55, Arg56 and Met57 from the γ loop are critical residues with respect to the different structures of

Figure 2

Stereoview of the PEG fragment (gray) in the final $2F_o–F_c$ electron-density map contoured at 1.0σ. Two adjacent FixJN molecules in the crystal (yellow and green) contribute to the binding of this fragment.

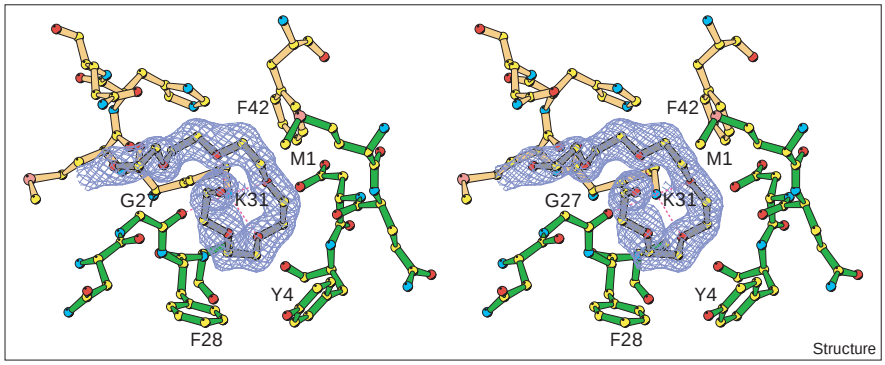

Figure 3

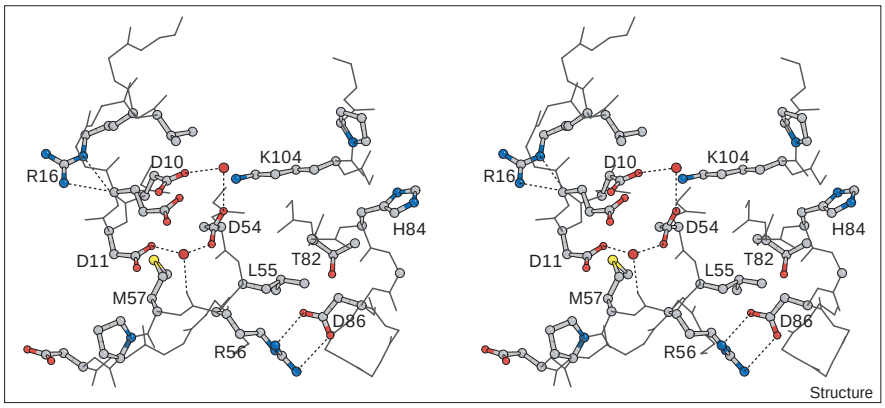

Stereoview of the active-site environment in the metal-free canonical structure. The water molecules are indicated by red spheres and the polar interactions by dotted lines. The color code for the atoms is oxygen in red, carbon in grey, nitrogen in blue and sulfur in yellow.

FixJN. The leucine and methionine sidechains are located in two hydrophobic pockets that line up the active site and define its geometry. The guanidinium group of Arg56 and the carboxylate group of Asp86 form electrostatic interactions that stabilize the conformation of the adjacent β4–α4 loop (residues 83–86) (Figure 3). In all metal-bound FixJN structures, the cation (Sm^{3+}, Mn^{2+} or Mg^{2+}) replaces the water molecule in the active site, and is liganded to the same protein atoms. Three water molecules fill out the octahedral coordination of the Mn^{2+} or Mg^{2+} ions (Figure 4). The distance of these ions to all ligands is 2.4 Å. The N terminus of helix α1 is stabilized by the hydrogen-bonding interaction between the mainchain oxygen of Asp10 and the guanidinium group of Arg16 (2.7 Å) (Figure 3).

The self-inhibited structure

The fold of the γ loop in this structure significantly alters the location and the conformation of several residues. Compared with the canonical structure, the C_α atom of Leu55 moves by 4.5 Å and this residue shifts from the α to the β conformation, which results in an extension of strand β3. The leucine sidechain is then located in the hydrophobic pocket previously occupied by the sidechain of Met57, which points into the solvent. As a consequence, the sidechain of Arg56 moves by 9 Å, runs across the metal-ion-binding site and fills the active site (Figure 5). In the triclinic structure solved at 1.6 Å resolution (Table 1), the guanidinium group forms a salt bridge and a hydrogen-bonding interaction with Glu12 (2.8 Å) and Asp54 (3.2 Å), respectively, and the ammonium group of Lys104 forms a salt-bridge interaction with Asp54 (2.9 Å) (Figure 5). Loops β4–α4 and β5–α5 are shifted by 0.9 Å, and the N terminus of helix α4 moves away from the protein core by about 1 Å, allowing hydrogen-bond formation between the carboxylate of Asp86 and the mainchain nitrogen atom of residue 89. Hatched electron density was observed in some protomers for residues 13–17 at the N terminus of helix α1. The perturbation in this region probably arises from the close proximity of the guanidinium group of Arg56 and the Val15 sidechain (3.3 Å) (Figure 5).

The atypical structure

The atypical structure of FixJN was found in one molecule of the asymmetric unit when monoclinic crystals were soaked with Mn^{2+} (Table 1). The fold of the γ loop

Figure 4

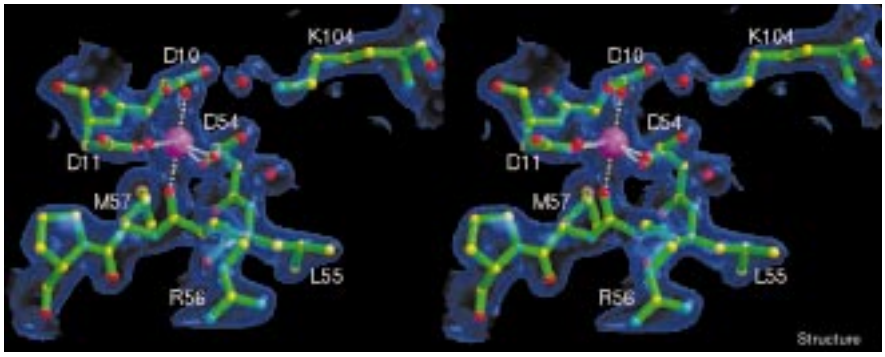

Stereoview of the active site in the Mn^{2+}-bound canonical structure of FixJN. The electron density is represented as a transparent solid, the water molecules as small red spheres and the Mn^{2+} as a large magenta sphere. Metal ion coordination bonds are illustrated by dotted lines.

Figure 5

Stereoview of the active-site environment in the self-inhibited FixJN structure. The water molecule is indicated by a red sphere and the polar interactions by dotted lines.

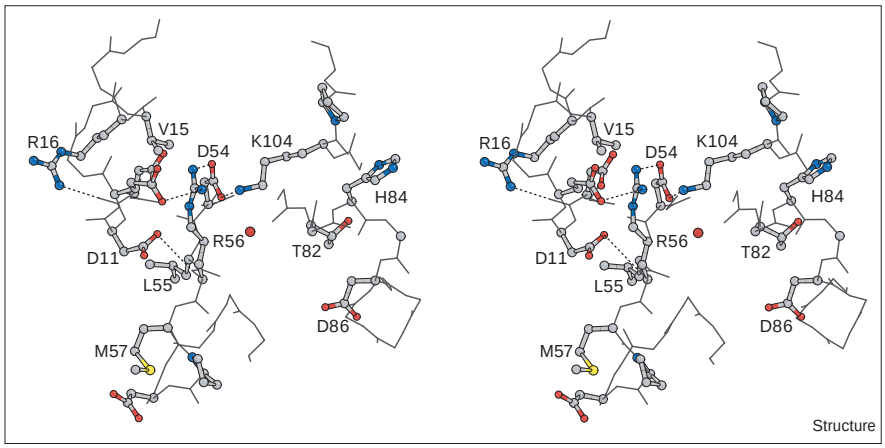

in the atypical structure is similar to the one of the self-inhibited structure with respect to the location of Leu55 and Met57 (Figure 6), but the conformation of the main-chain atoms of residues 56–61 differs by an rmsd value of 1.7 Å. The absence of electron density for Arg56 from the C_β atom suggests that the guanidinium group is no longer anchored to the active-site residues. In this structure, unwinding of the N terminus of helix α1 (residues 13–17) occurs and brings the C_α atom of the strongly conserved Arg16 8 Å away from its position in the self-inhibited and canonical structures (Figure 6). The invariant aspartic acids (Asp11 and Asp54) do not constitute an acidic pocket suitable for metal binding.

Molecular indicators of the conformational states of FixJN

The N terminus of helix α1, and the loops β1–α1, β3–α3 and β4–α4 define the active-site area of the receiver domain. The atypical structure, where the N-terminal part of helix α1 unwinds up to Ser18, has never been observed in the crystal structures of isolated receiver domains, but motions of this region have been described in Spo0F [30,31], and unfolding of the first turn of helix α1 occurred in CheY in complex with the phosphotransfer domain of ArcB [32]. This structure of FixJN was found when the crystals were soaked with Mn^{2+}, a cation present at high concentrations in the nodules on the plant roots where *S. meliloti* resides [7]. The atypical structure may illustrate a folding intermediate from the self-inhibited to the canonical structures, but the possibility that functional aspects may be related to this structure cannot be ruled out. Indeed, the residues that most severely influence the protein–protein interactions for phosphotransfer between Spo0F and Spo0B are located in the region of helix α1 that unwinds in FixJN [33].

Figure 6

Stereoview of the superposed atypical structure (mainchain atoms in green; filled sidechain bonds) and self-inhibited structure (mainchain atoms in black; open sidechain bonds).

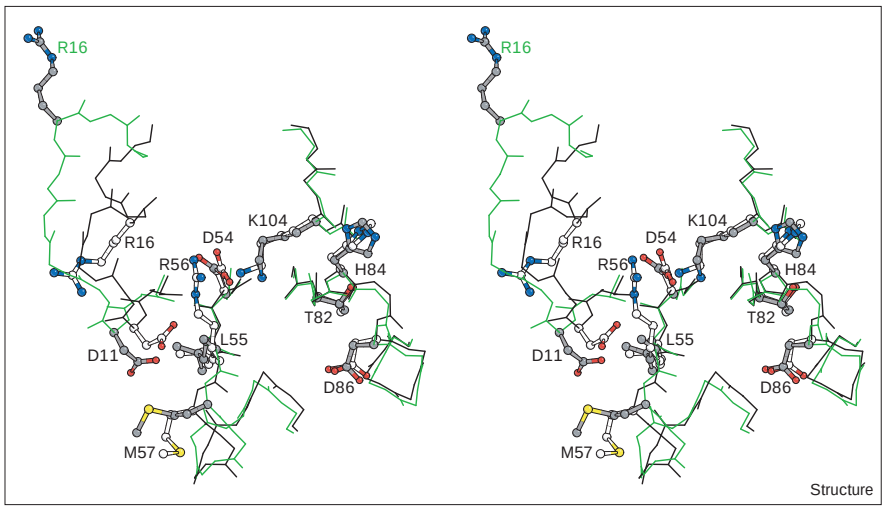

Figure 7

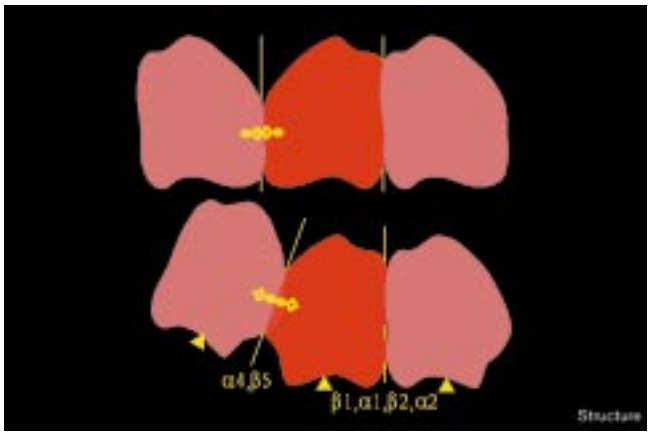

Cartoon representing the protein–protein interfaces mediated by twofold axes (yellow vertical lines) in the crystals for unphosphorylated FixJN (top) and phosphorylated FixJN (bottom). The β1–α1–β2–α2 interface is not affected by the phosphorylation state of the protein. The α4–β5 interface mediates dimerization of the receiver domain after the phosphorylation-induced conformational change of the contact area. The triangles point to the active site and the symbol at the α4–β5 interface represents the invariant aromatic residue (Phe101 in FixJ). It is oriented towards the solvent in each unphosphorylated FixJN protomer and towards the protomer core in the phosphorylated species.

The β3–α3 loop (γ loop, residues 55–61) is edged by two invariant residues, the phosphorylatable Asp54 and Gly62, and the residues found at positions 55 and 57 are hydrophobic in all response regulator proteins [19]. This loop delineates one side of the acidic pocket, and provides one of the three protein ligands (the mainchain oxygen atom of residue 56) to the essential metal ion. The conformation of the γ loop observed in the self-inhibited FixJN structure is unprecedented with respect to the location of the Leu55 and Arg56 residues. The Arg56 sidechain enters the active site and the strong polar interactions that are established suggest that the β3–α3 loop may act as a molecular switch for auto-inhibition of the receiver domain. Reports on other response regulator proteins indicate that this property may not be unique to FixJ. The flexibility of the β3–α3 loop in CheY from *E. coli* and in Spo0F from *Bacillus subtilis* was observed by nuclear magnetic resonance (NMR) spectroscopy studies [31,34]. Two conformations of this loop were also observed in the crystal structures of the metal-free PhoB from *E. coli* [26] and CheY from *Thermotoga maritima* [35]. In the latter protein, one conformation of the β3–α3 loop brings the Thr56 sidechain within hydrogen-bonding distance of Asp54 and precludes phosphorylation. The same consequence holds in CheB and NarL where the sidechains of the equivalent residues, Glu58 and Asn61, respectively, are hydrogen bonded to the phosphorylatable aspartic acid [23,25]. From the collective X-ray and NMR data it would seem that receiver domains may present a significant population of conformers impaired to different extents and in different ways for catalysis. Their occurrence may account, for example, for the high dissociation constant for divalent cations in Spo0F, which led to the proposal that the uncomplexed form might be the predominant biological state [24]. The stability of these metal-free conformers may possibly depend on the residue type within this loop region and contribute, in each system, to a subtle tuning of the regulation of signal transduction.

In the canonical structure of FixJN, the conformation of the β3–α3 loop not only excludes the Arg56 sidechain from the active site but also allows the formation of a salt-bridge

Figure 8

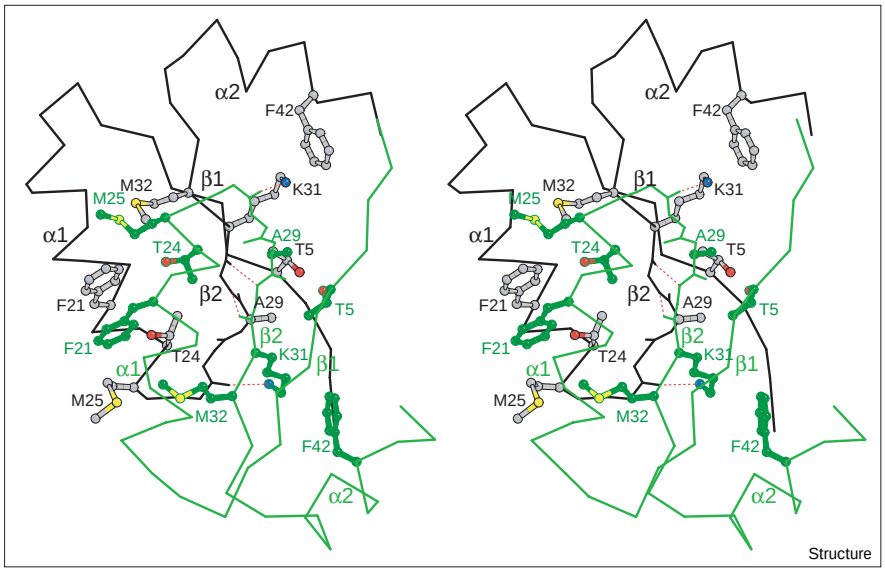

Stereoview of the β1–α1–β2–α2 interface found in the FixJN crystals. The C_α traces of two protomers are shown in green and black, respectively. The FixJN molecules are related by a twofold axis nearly horizontal in the plane of the figure. Two symmetrical hydrogen bonds are exchanged between the mainchain atoms of residues 30 in the adjacent β2 strands. Two hydrogen bonds are formed between the amino group of Lys31 and the mainchain oxygen atom of residue 27. The PEG fragment (see Figure 2) is bound in the vicinity of this interface region.

interaction between Arg56 and Asp86 from the β4–α4 loop. This interaction stabilizes the conformation of the β4–α4 loop and, in turn, the structure of the pre-phosphorylation state of the receiver domain [13]. This interaction is broken in phospho-FixJN as a consequence of the phosphorylation-induced large conformational change of the β4–α4 loop [13]. It therefore seems that the conformations of both the β3–α3 and β4–α4 loops may act as molecular indicators of the FixJN receiver domain to define the self-inhibited, the canonical unphosphorylated or the phosphorylated states. In these three structures, the fold of the β1–α1 loop and of the N-terminal part of helix α1 are identical (Figure 3,5) [13].

Protein interfaces as modulators of the functional states

The transition from the canonical to the self-inhibited structure, induced by the binding of $PtCl_4^{2-}$ 30 Å away from the active site, cannot be predicted from the structure. It nevertheless suggests that the conformational state (self-inhibited or canonical) of the unphosphorylated receiver domain may be influenced by binding interactions in the receiver domain, at a remote distance from the active site. This transition between two conformational states and the solving of a self-inhibited structure of FixJN offer a possible explanation for the 44-fold inhibition of phosphorylation of the receiver domain by the C-terminal domain in the full-length response regulator [12]. The protein–protein interface between these domains is known to mediate the inhibition of the DNA-binding properties of the C-terminal domain [11]. The hypothesis that this protein–protein interface may have a dual function and favor the self-inhibited structure of the receiver domain is attractive because it would be a means of protecting the response regulator, *in vivo*, against fortuitous phosphorylation by small phosphodonnors [36] and unrelated kinases.

Another modulation of the function in response regulator proteins is the formation of oligomeric species induced by phosphorylation but also favored upon binding to the DNA targets, which may potentiate protein–protein interactions by increasing the local concentration of the proteins [37]. Crystal-packing constraints, by promoting intermolecular associations, may suggest protein–protein interfaces of biological significance. Two contact areas between FixJN protomers were found in both monoclinic and triclinic crystals. The first protein–protein interface excludes 700 Å^2 from the solvent, and involves residues from helix α4 and strand β5 from each protomer. This interface does not lead to dimeric FixJN species in solution but the phosphorylation-induced conformational changes in this region restructure the protomer surface, allow a new orientation of the molecules and increase the contact area to 900 Å^2 (Figure 7). This α4–β5 interface mediates dimerization of phosphorylated FixJN as well as that of the phosphorylated full-length protein, which significantly increases the binding of the response regulator to the *fixK* promoter [12,13].

A second interface between FixJN molecules is located 30 Å away and involves 20 residues from helix α1, strand β2 and helix α2 from each protomer. It is is mostly hydrophobic and excludes 1,700 Å^2 from solvent (Figure 8). This value is significant and, in the crystal, this interface associates FixJN molecules independent of their phosphorylation state. This favorable area may promote the formation of oligomeric forms of FixJ, *in vivo*, as was suggested to occur for NarL, PhoP, OmpR, and VirG [38–41] and shown for UphA and NtrC [42,43] when these proteins bind to their target promoters.

Four significantly different conformations of the receiver domain of FixJ are now documented. One of them illustrates the phosphorylated state, and the three others were found for the unphosphorylated protein. These structures differ by the conformation of all regions lining the active site, the β1–α1 loop and the N-terminal part of helix α1, the β3–α3 and the β4–α4 loops. Interestingly, alanine-scanning mutagenesis on Spo0F recently showed that three groups of residues located in these regions define the molecular surfaces for the specific recognition of this response regulator with its phosphorelay proteins [33,44,45]. Mutational, biochemical and genetic studies are underway to identify the residues essential for the FixL/FixJ interactions and to address the biological significance of the α1–β2–α2 interface.

Biological implications

Two-component systems mediate a large variety of adaptative cellular responses to environmental stimuli in bacteria. The FixL/FixJ system is responsible for the regulation of nitrogen-fixation genes in *S. meliloti,* symbiotic bacteria that are responsible for the formation of, and reside in, nodules on plant roots that enable nitrogen to be provided to the plant. In microaerobic conditions, autophosphorylation of the kinase FixL and phosphotransfer to the receiver domain of FixJ activates the transcription of more than twenty genes. Activation of the response regulator proteins by the kinases in two-component systems involves a metal-ion-dependent mechanism and a specific recognition of the two protein partners in order to minimize detrimental cross-talk between unrelated signaling cascades. The seven X-ray structures of the unphosphorylated N-terminal receiver domain of FixJ (FixJN) solved in this study, with and without bound metal cations, illustrate three conformations of the unphosphorylated receiver domain and shed some light on possible regulatory aspects of this activation.

One of these structures is impaired for catalysis. This feature is not unique to this receiver domain but in FixJ it involves a major conformational change of the β3–α3

loop. It may be favored in the full-length FixJ protein by interactions or topological constraints between the receiver domain and the C-terminal DNA-binding domain. This hypothesis would provide an explanation for the kinetics of phosphorylation of FixJ, and, *in vivo*, would constitute an attractive way of minimizing fortuitous activation of the response regulator protein by phosphodonnors other than the cognate kinase.

The second FixJN structure displays the standard geometry of the active site. This canonical form was found in the absence and in the presence of bound catalytic metal ions, suggesting that the canonical form would be a precursor rather than a product of metal binding. From this set of structures and the X-ray and NMR data on homologous proteins, it would seem that factors modulating the stability of the metal-free conformers of response regulator proteins may provide a subtle tuning for the regulation of their activation.

In the structures of unphosphorylated FixJN reported here, significant conformational changes are observed in the β1–α1 loop, the N-terminal part of helix α1, and the β3–α3 loop. The third loop in the active-site area, β4–α4, undergoes a large movement upon phosphorylation of the receiver domain [13]. This ensemble of crystal structures corresponds to two signaling states (unphosphorylated and phosphorylated) and, within the unphosphorylated state, to apparently different functional states — impaired and ready for catalysis. Each of these structures offers different potential recognition surfaces to the FixL protein because of the conformations of these loops.

The intermolecular associations found between FixJN protomers in these crystal structures involve two distinct regions, the β4–α5 and the β1–α2–β2 surfaces. Dimerization of FixJ via the β4–α5 region [13] and further oligomerization, possibly mediated by the β1–α2–β2 interface, would be in line with the protection of about 50 base pairs on the DNA promoter region of *fixK* [15].

Materials and methods

Crystallization and data collection

The FixJN protein (residues 1–126) was expressed from the pTF7-7 plasmid in the *E. coli* strain BL21(DE3)(pLysS). The protein was purified to homogeneity using chromatographic methods [13]. FixJN monomer in 20 mM Tris-HCl (pH 7.0), 0.1 mM EDTA, 1 mM dithiothreitol (DTT) was concentrated to 12 mg ml^{-1} using Centricon 10. Crystals were grown at 4°C using the hanging-drop vapor-diffusion method.

Triclinic crystals were obtained by mixing the protein solution (2 µl) with an equal volume of the reservoir solution, which contained 40% (w/v) polyethylene glycol (PEG) 1500 in 20 mM Tris buffer (pH 7.0). After three months, the crystal dimensions were about $150 \times 50 \times 20\ \mu m^3$. The crystals have unit-cell dimensions a = 31.7 Å, b = 42.2 Å, c = 44.6 Å, α = 93.2°, β = 104.5° and γ = 101.9°, and contain two molecules per asymmetric unit for a solvent content of 30%. Monoclinic crystals were obtained by mixing the protein solution (2 µl) with an equal volume of the reservoir solution, which contained 40% w/v PEG 1500 in 100 mM Tris buffer (pH 7.8). After five months, the crystal dimensions were about $100 \times 20 \times 20\ \mu m^3$. The space group is C2 and the cell parameters are a = 114.4 Å, b = 36.2 Å, c = 66.4 Å, β = 117.6°. There are two molecules in the asymmetric unit for a solvent content of 40%. Heavy-atom derivatives were obtained by soaking triclinic crystals in a 4 mM $Sm(NO_3)_3$ solution for 48 h, or in a 8 mM K_2PtCl_4 solution for 15 h (Table 2). Mn^{2+} and Mg^{2+} derivatives were obtained by soaking monoclinic crystals in 5 mM $MnCl_2$ for 24 h, and triclinic crystals in 20 mM $MnCl_2$ for 43 h or in 20 mM $MgCl_2$ for 23 h.

Triclinic and monoclinic crystals were cryocooled in liquid propane and stored at liquid-nitrogen temperature. The data sets were collected at 95K on synchrotron beam lines W32 at LURE (Orsay), and D2AM, ID14-EH3 and ID14-EH4 at ESRF (Grenoble). Data processing was performed using DENZO and SCALEPACK (Table 2) [46].

Structure determinations: triclinic forms

Attempts to solve the structure by molecular replacement using the coordinates of homologous domains (CheY, Spo0F, NtrC, NarL, CheB) as a model were unsuccessful. The native, Sm^{3+} and $PtCl_4^{2-}$ data sets were used for phasing at 2.4 Å resolution. Four heavy-atom sites were located in each derivative by inspection of Patterson and Fourier difference maps. Phasing was performed using SHARP [47] and took into account the anomalous signal of the Sm^{3+} derivative (Table 2). The initial figure of merit was 0.52. Cycles of solvent flattening and histogram matching were performed with DM [48] using a solvent mask generated automatically. The position of the noncrystallographic twofold axis, detected by calculation of a self-rotation function using the program POLARRFN of the CCP4 suite [48], was determined from the improved phases using GETAX [49]. The real-space correlation coefficient (Cc) was 34% at 4 Å resolution. Subsequent cycles of density modification using noncrystallographic-symmetry averaging improved the value of Cc to 90% at 2.4 Å resolution. The initial atomic model was generated from the $2F_o–F_c$ electron-density map. This model was used to calculate a new mask using MAMA [50]. Further cycles of density modification led to a map of excellent quality in which a new model containing 112 residues was built.

Refinement was performed using data at the highest available resolution for each crystal species (Table 1). Refinement included cycles of conjugate gradient minimisation and molecular dynamics using CNS [51]. Bulk-solvent correction and noncrystallographic symmetry (NCS) constraints were applied. The cross-validation factor, R_{free}, was evaluated using 10% of the data set. NCS restraints were applied when the R and R_{free} values dropped to 28% and 32%, respectively. In the last stages of refinement, the two copies in the asymmetric unit were refined independently, solvent molecules were positioned and restrained individual B factors were calculated. For the native triclinic crystals, the final R and R_{free} values at 1.6 Å resolution were 18.7% and 22.4%, respectively (Table 1). In copy A of the asymmetric unit (named self-inhibited in Table 1), no electron density could be assigned for residues 13–17, and 57–59. The second copy, B (named canonical in Table 1), is fully defined from residues 1–125. A few sidechains had no electron density from the C_α positions (Glu13A, Val15A, Met57A) or from their C_β positions (Gln34A, Arg67A, Glu64B and Arg67B). The sidechains of residues Met25A, Ser78A, Ser18B, Val50B, Ser78B and Ile102B have been modeled as two-state conformers. Residue 105 is a *cis*-proline. 148 water molecules and a hydroxycarbonated chain of 19 atoms have been positioned. This chain has been interpreted as a fragment of PEG 1500. The average temperature factors are 23 $Å^2$ for copy A, 20 $Å^2$ for copy B, 30 $Å^2$ for water molecules and 22 $Å^2$ for the PEG fragment. A Ramachandran plot generated with PROCHECK [52] locates 95% of the residues in the most-favored regions.

The structures of the $PtCl_4^{2-}$, Sm^{3+}, Mn^{2+} and Mg^{2+} derivatives of FixJN in triclinic crystals were refined as described above, using the native structure of the protein as starting model. In the $PtCl_4^{2-}$

Table 2

Data collection and statistics.

Crystal form	Triclinic							Monoclinic	
Data	Native 1	Native 2	Merge	$Sm(NO_3)_3$	K_2PtCl_4	$MnCl_2$	$MgCl_2$	Native	$MnCl_2$
Resolution (Å)	2.4	1.6	1.6	2.4	1.9	2.0	2.0	2.9	3.0
Wavelength (Å)	0.93	0.95	-	0.93	0.93	0.95	0.95	1.07	0.95
Oscillation (step°)	180 (1)	247.5 (2.5)	-	300 (3)	180 (1)	172.5 (2.5)	240 (2.5)	180 (2.5)	196.5 (1.5)
No. of measurements	15,435	48,916	62,615	26,081	30,758	24,325	31,730	15,742	14,984
No. of uniques	8231	19,484	20,628	8265	15,980	13,062	13,586	5471	4760
Completeness (%)	98	66*	73*	98	94	87	88	97	97
$I > 3\sigma(I)$ (%)	95	64	70	93	80	74	96	87	91
R_{sym} (%)	2.1	6.6	7.1†	5.0	4.0	5.1	8.7	7.7	6.0
R_{iso} (%)	-	-	-	27	29	30	25	-	47
R_{cullis} (iso/ano)	-	-	-	0.8/0.6	0.9/-	-	-	-	-
Power‡ (iso/ano)	-	-	-	1.5/1.8	1.1/-	-	-	-	-

$R_{sym} = \Sigma \left| I - < I > \right| / \Sigma I$. *Completeness is 95% to 1.9 Å, †R_{merge}. ‡Phasing power. Unit-cell dimensions are a = 31.7 Å, b = 42.2 Å, c = 44.6 Å, α = 93.2°, β = 104.5°, γ= 101.9° for the triclinic form; and a = 114.4 Å, b= 36.2 Å, c = 66.4 Å, β = 117.6° for the monoclinic form.

derivative, the two copies in the asymmetric unit are identical and adopt the self-inhibited conformation (Table 1). The two molecules in the asymmetric units of the Sm^{3+}, Mn^{2+} and Mg^{2+} derivatives are identical and adopt the canonical conformation (Table 1).

Structure determinations: monoclinic forms.

The structure of FixJN in the triclinic crystals was used to solve the structure of the protein in the native and in the Mn^{2+}-soaked monoclinic crystals. A unique solution was found by molecular replacement using the program AMoRe [53] for two copies in the asymmetric unit. Refinement was conducted as described for the triclinic form but the NCS restraints (weight = 100 kcal mol^{-1} $Å^{-2}$) were kept throughout refinement because of the lower resolution limit. In native crystals, the two copies in the asymmetric unit are similar and are found in the self-inhibited conformation. In Mn^{2+}-soaked crystals, the two copies have different conformations. One monomer adopts the canonical fold with a Mn^{2+} ion bound in the active site and the second monomer is found in a new conformation named 'atypical' (Table 1). The electron density for residues 13–17 is continuous but does not allow an accurate model building for the mainchain atoms. The average temperature factor, 59 $Å^2$, is high for this derivative, as was the value calculated from a Wilson plot (72 $Å^2$).

Electron-density maps were displayed on a Silicon Graphics workstation using TURBO-FRODO [54]. Secondary structure assignments and solvent accessibilities were calculated with DSSP [55]. Atomic models were superposed using LSQKAB of the CCP4 suite [48].

Accession numbers

The coordinates of the self-inhibited, canonical and atypical structures have been deposited with the PDB with accession codes 1DBW, 1DCK and 1DCM, respectively.

Acknowledgements

We thank the scientific staff of LURE (Orsay, France) and ESRF (Grenoble, France) for excellent data collection facilities, and E Courcelle for computing facilities. This work was supported by grants from the European Union (BIO4 CT97-2143) and the Ministère de l'Education Nationale, de la Recherche et de la Technologie (Programme de Recherche Fondamentale en Microbiologie et Maladies Infectieuses et Parasitaires).

References

1. Stock, J.B., Stock, A.M. & Mottonen, J.M. (1990). Signal transduction in bacteria. *Nature* **344**, 395-400.
2. Parkinson, J.S. & Kofoid, E.C. (1992). Communication modules in bacterial signaling proteins. *Annu. Rev. Genet.* **26**, 71-112.
3. Parkinson, J.S. (1993). Signal transduction schemes of bacteria. *Cell* **73**, 857-871.
4. Appleby, J.L., Parkinson, J.S. & Bourret, R.B. (1996). Signal transduction via the multistep phosphorelay: not necessarily a road less traveled. *Cell* **86**, 845-848.
5. Mizuno, T. (1998). His-Asp phosphotransfer signal transduction. *J. Biochem.* **123**, 555-563.
6. David, M., *et al.*, & Kahn, D. (1988). Cascade regulation of gene expression in *Rhizobium meliloti*. *Cell* **54**, 671-683.
7. Agron, P.G. & Helinski, D.R. (1995). Symbiotic expression of *Rhizobium meliloti* nitrogen fixation genes is regulated by oxygen. In *Two-Component Signal Transduction* (Hoch, J.A. & Silhavy, T., eds), pp 275-287, ASM Press, Washington D.C.
8. Roberts, D.L., Bennett, D.W. & Forst, S.A. (1994). Identification of the site of phosphorylation on the osmosensor, EnvZ, of *Escherichia coli*. *J. Biol. Chem.* **269**, 8728-8733.
9. Bilwes, A.M., Alex, L.A., Crane, B.R. & Simon, M.I. (1999). Structure of CheA, a signal-transducing histidine kinase. *Cell* **96**, 131-141.
10. Kahn, D. & Ditta, G. (1991). Modular structure of FixJ: homology of the transcriptional activator domain with the -35 binding domain of sigma factors. *Mol. Microbiol.* **5**, 987-997.
11. Da Re, S., Bertagnoli, S., Fourment, J., Reyrat, J.-M. & Kahn, D. (1994). Intramolecular signal transduction within the FixJ transcriptional activator: *in vitro* evidence for the inhibitory effect of the phosphorylatable regulatory domain. *Nucleic Acids Res.* **22**, 1555-1561.
12. Da Re, S., Schumacher, J., Rousseau, P., Fourment, J., Ebel, C. & Kahn, D. (1999). Phosphorylation-induced dimerisation of the FixJ receiver domain. *Mol. Microbiol.*, **34**, 504-511.
13. Birck, C., *et al.*, & Samama, J.P. (1999). Conformational changes induced by phosphorylation of the FixJ receiver domain. *Structure* **7**, 1505-1515.
14. Agron, P.G., Ditta, G.S. & Helinski, D.R. (1993). Oxygen regulation of *nifA* transcription *in vitro*. *Proc. Natl Acad. Sci. USA* **90**, 3506-3510.
15. Galinier, A., Garnerone, A.M., Reyrat, J.M., Kahn, D., Batut, J. & Boistard, P. (1994). Phosphorylation of the *Rhizobium meliloti* FixJ protein induces its binding to a compound regulatory region at the *fixK* promoter. *J. Biol. Chem.* **269**, 23784-23789.
16. Reyrat, J.M., David, M., Blonski, C., Boistard, P. & Batut, J. (1993). Oxygen-regulated in vitro transcription of *Rhizobium meliloti nifA* and *fixK* genes. *J. Bacteriol.* **175**, 6867-6872.

17. Lukat, G.S., Stock, A.M. & Stock, J.B. (1990). Divalent metal ion binding to the CheY protein and its significance to phosphotransfer in bacterial chemotaxis. *Biochemistry* **29**, 5436-5442.
18. Stock, A.M., *et al*., & Petsko, G.A. (1993). Structure of the Mg(2+)-bound form of CheY and mechanism of phosphoryl transfer in bacterial chemotaxis. *Biochemistry* **32**, 13375-13380.
19. Volz, K. (1993). Structural conservation in the CheY superfamily. *Biochemistry* **32**, 11741-11753.
20. Bellsolell, L., Prieto, J., Serrano, L. & Coll, M. (1994). Magnesium binding to the bacterial chemotaxis protein CheY results in large conformational changes involving its functional surface. *J. Mol. Biol.* **238**, 489-495.
21. Volkman, B.F., Nohaile, M.J., Amy, N.K., Kustu, S. & Wemmer, D.E. (1995). Three-dimensional solution structure of the N-terminal receiver domain of NTRC. *Biochemistry* **34**, 1413-1424.
22. Feher, V.A., Zapf, J.W., Hoch, J.A., Dahlquist, F.W., Whiteley, J.M. & Cavanagh, J. (1995). 1H, 15N, and 13C backbone chemical shift assignments, secondary structure, and magnesium-binding characteristics of the *Bacillus subtilis* response regulator, Spo0F, determined by heteronuclear high-resolution NMR. *Protein Sci.* **4**, 1801-1814.
23. Baikalov, I., Schroder, I., Kaczor-Grzeskowiak, M., Grzeskowiak, K., Gunsalus, R.P. & Dickerson, R.E. (1996). Structure of the *Escherichia coli* response regulator NarL. *Biochemistry* **35**, 11053-11061.
24. Madhusudan, M., Zapf, J., Hoch, J.A., Whiteley, J.M., Xuong, N.H. & Varughese, K.I. (1997). A response regulatory protein with the site of phosphorylation blocked by an arginine interaction: crystal structure of Spo0F from *Bacillus subtilis*. *Biochemistry* **36**, 12739-12745.
25. Djordjevic, S., Goudreau, P.N., Xu, Q., Stock, A.M. & West, A.H. (1998). Structural basis for methylesterase CheB regulation by a phosphorylation-activated domain. *Proc. Natl Acad. Sci. USA* **95**, 1381-1386.
26. Solà, M., Gomis, F., Serrano, L., Gonzalez, A. & Coll, M. (1999). Three-dimensional crystal structure of the transcription factor PhoB receiver domain. *J. Mol. Biol.* **285**, 675-687.
27. Chevrier, B., Moras, D., Behr, J.P. & Lehn, J.M. (1987). Structure of the hydrazinium complex of a tetracarboxy-18-crown-6 receptor molecule. *Acta Crystallogr. C* **43**, 2134-2137.
28. Becker, A., Schlichting, I., Kabsch, W., Schultz, S. & Wagner, A.F. (1998). Structure of peptide deformylase and identification of the substrate binding site. *J. Biol. Chem.* **273**, 11413-11416.
29. Ranganathan, R., Lu, K.P., Hunter, T. & Noel, J.P. (1997). Structural and functional analysis of the mitotic rotamase Pin1 suggests substrate recognition is phosphorylation-dependent. *Cell* **89**, 875-886.
30. Feher, V.A., *et al*., & Cavanagh, J. (1997). High-resolution NMR structure and backbone dynamics of the *Bacillus subtilis* response regulator, Spo0F: implications for phosphorylation and molecular recognition. *Biochemistry* **36**, 10015-10025.
31. Feher, V.A. & Cavanagh, J. (1999). Millisecond-timescale motions contribute to the function of the bacterial response regulator protein Spo0F. *Nature* **400**, 289-293.
32. Kato, M., Shimizu, T., Mizuno, T. & Hakoshima, T. (1999). Structure of the histidine-containing phosphotransfer (HPt) domain of the anaerobic sensor protein ArcB complexed with the chemotaxis response regulator CheY. *Acta Crystallogr. D* **55**, 1257-1263.
33. Tzeng, Y.L. & Hoch, J.A. (1997). Molecular recognition in signal transduction: the interaction surfaces of the Spo0F response regulator with its cognate phosphorelay proteins revealed by alanine scanning mutagenesis. *J. Mol. Biol.* **272**, 200-212.
34. Moy, F.J., Lowry, D.F., Matsumura, P., Dahlquist, F.W., Krywko, J.E. & Domaille, P.J. (1994). Assignments, secondary structure, global fold, and dynamics of chemotaxis Y protein using three- and four-dimensional heteronuclear (13C,15N) NMR spectroscopy. *Biochemistry* **33**, 10731-10742.
35. Usher, K.C., de la Cruz, A.F., Dahlquist, F.W., Swanson, R.V., Simon, M.I. & Remington, S.J. (1998). Crystal structures of CheY from *Thermotoga maritima* do not support conventional explanations for the structural basis of enhanced thermostability. *Protein Sci.* **7**, 403-412.
36. McCleary, W.R. & Stock, J.B. (1994). Acetyl phosphate and the activation of two-component response regulators. *J. Biol. Chem.* **269**, 31567-31572.
37. Rippe, K., Mucke, N. & Schulz, A. (1998). Association states of the transcription activator protein NtrC from *E. coli* determined by analytical ultracentrifugation. *J. Mol. Biol.* **278**, 915-933.
38. Baikalov, I., Schroder, I., Kaczor-Grzeskowiak, M., Cascio, D., Gunsalus, R.P. & Dickerson, R.E. (1998). NarL dimerization? Suggestive evidence from a new crystal form. *Biochemistry* **37**, 3665-3676.
39. Liu, W. & Hulett, F.M. (1997). *Bacillus subtilis* PhoP binds to the phoB tandem promoter exclusively within the phosphate starvation-inducible promoter. *J. Bacteriol.* **179**, 6302-6310.
40. Nakashima, K., Kanamaru, K., Aiba, H. & Mizuno, T. (1991). Signal transduction and osmoregulation in *Escherichia coli*. A novel type of mutation in the phosphorylation domain of the activator protein, OmpR, results in a defect in its phosphorylation-dependent DNA binding. *J. Biol. Chem.* **266**, 10775-10780.
41. Powell, B.S. & Kado, C.I. (1990). Specific binding of VirG to the vir box requires a C-terminal domain and exhibits a minimum concentration threshold. *Mol. Microbiol.* **4**, 2159-2166.
42. Webber, C.A. & Kadner, R.J. (1997). Involvement of the amino-terminal phosphorylation module of UhpA in activation of uhpT transcription in *Escherichia coli*. *Mol. Microbiol.* **24**, 1039-1048.
43. Wyman, C., Rombel, I., North, A.K., Bustamante, C. & Kustu, S. (1997). Unusual oligomerization required for activity of NtrC, a bacterial enhancer-binding protein. *Science* **275**, 1658-1661.
44. Tzeng, Y.L., Feher, V.A., Cavanagh, J., Perego, M. & Hoch, J.A. (1998). Characterization of interactions between a two-component response regulator, Spo0F, and its phosphatase, RapB. *Biochemistry* **37**, 16538-16545.
45. Jiang, M., Tzeng, Y.L., Feher, V.A., Perego, M. & Hoch, J.A. (1999). Alanine mutants of the Spo0F response regulator modifying specificity for sensor kinases in sporulation initiation. *Mol. Microbiol.* **33**, 389-395.
46. Otwinowski, Z.O. & Minor, W. (1997). Processing of X-ray diffraction data collected in oscillation mode. *Methods Enzymol.* **276**, 307-326.
47. de La Fortelle, E. & Bricogne, G. (1997). Maximum-likelihood heavy-atom parameter refinement for multiple isomorphous replacement and multiwavelength anomalous diffraction methods. *Methods Enzymol.* **276**, 472-494.
48. Collaborative Computational Project, Number 4. (1994). The CCP4 suite: programs for protein crystallography. *Acta Crystallogr. D* **50**, 760-763.
49. Vonrhein, C. & Schulz, G.E. (1999). Locating proper non-crystallographic symmetry in low-resolution electron-density maps with the program GETAX. *Acta Crystallogr. D* **55**, 225-229.
50. Kleywegt, G.J. & Jones, T.A. (1993). In *Joint CCP4 and ESF-EACBM Newsletter on Protein Crystallography* Vol. 28, pp. 56–59. SERC Daresbury Laboratory, Warrington, UK.
51. Brünger, A.T., *et al*., & Warren, G.L. (1998). Crystallography & NMR system: a new software suite for macromolecular structure determination. *Acta Crystallogr. D* **54**, 905-921.
52. Laskowski, R.A., MacArthur, M.W., Moss, D.S. & Thornton, J.M. (1993). PROCHECK: a program to check the stereochemical quality of protein structures. *J. Appl. Crystallogr.* **26**, 283-291.
53. Navaza, J. & Saludjian, P. (1997). AMoRe: an automated molecular replacement program package. *Methods Enzymol* **276**, 581-594.
54. Roussel, A. & Cambillau, C. (1989). TURBO-FRODO. In *Silicon Graphics Geometry Partner Directory* (Silicon Graphics, ed.), pp 71-78, Silicon Graphics, Mountain View, CA.
55. Kabsch, W. & Sander, C. (1983). Dictionary of protein secondary structure: pattern recognition of hydrogen-bonded and geometrical features. *Biopolymers* **22**, 2577-2637.
56. Volz, K. & Matsumura, P. (1991). Crystal structure of *Escherichia coli* CheY refined at 1.7 Å resolution. *J. Biol. Chem.* **266**, 15511-15519.
57. Gouet, P., Courcelle, E., Stuart, D. & Metoz, F. (1998). ESPript: multiple sequence alignments in PostScript. *Bioinformatics* **15**, 305-308.